Available online at www.sciencedirect.com
SCIENCE DIRECT®
Thermochimica Acta 426 (2005) 39–48
thermochimica acta
www.elsevier.com/locate/tca

Synthesis of strontium bismuth niobate ($SrBi_2Nb_2O_9$) using an aqueous acetate–citrate precursor gel: thermal decomposition and phase formation

D. Nelis[a], D. Mondelaers[a,b], G. Vanhoyland[a], A. Hardy[a], K. Van Werde[a], H. Van den Rul[a,b], M.K. Van Bael[a], J. Mullens[a,*], L.C. Van Poucke[a], J. D'Haen[b]

[a] *Laboratory of Inorganic and Physical Chemistry-IMO, Limburgs Universitair Centrum, Universitaire Campus, Building D, B-3590 Diepenbeek, Belgium*
[b] *IMO - IMOMEC, Limburgs Universitair Centrum, B-3590 Diepenbeek, Belgium*

Received 31 December 2003; accepted 12 July 2004
Available online 11 September 2004

Abstract

An aqueous solution–gel route was developed for the preparation of the ferroelectric material strontium bismuth niobate ($SrBi_2Nb_2O_9$, SBN). Starting from aqueous Bi^{3+}-acetate and Sr^{2+}-acetate solutions and an aqueous peroxo-citrato-Nb^{5+}-precursor solution, this method offers a low-cost and environmentally friendly alternative to the conventional sol–gel techniques. With regard to the deposition of thin films, it is important to gain insight in the behaviour of the precursor during thermal treatment. For this reason the thermal decomposition mechanism of the precursor gel was studied: weight loss and evolved gases were characterized by (hyphenated) TGA–MS and TGA–FTIR, while changes in the solid state during heating were detected using high temperature diffuse reflectance infrared fourier transform spectroscopy (HT-DRIFT). The decomposition in dry air can be divided in four temperature regions. The first two steps are ascribed to the drying of the sample and to the decomposition of the organic matrix, not coordinated to the metal ions. During the third step the coordination sphere of the metal ions is decomposed and finally the residual organic matter is combusted in the fourth region.

TEM experiments on freestanding thin films showed that the precursor homogeneity was maintained throughout the entire thermo-oxidative decomposition of the gel.

The phase formation of SBN was studied by means of high temperature X-ray diffraction (HT-XRD). At about 425 °C the intermediate fluorite phase is crystallized out of the amorphous precursor. The phase transformation into the desired ferroelectric perovskite phase seems to be dependent on the Bi-content: an excess of Bi lowers the onset temperature of perovskite formation.

Keywords: Sol–gel processes; Strontium bismuth niobate (SBN); Phase formation; Thermal decomposition; TGA–EGA

1. Introduction

During the last decade a lot of research has been carried out on the so-called Bi-based layer-structured ferroelectric oxides (BLSF) since these materials are excellent candidates for application as nonvolatile ferroelectric random access memory (NVFRAM). Important advantages of the BLSF-materials are the resistance to polarization fatigue up to 10^{12} cycles of polarization, the excellent retention properties and the low leakage currents on Pt electrodes, even for very thin films (ultra-thin films with thickness lower than 100 nm) [1]. The Bi-layered perovskites belong to the Aurivillius family and can be described by the general formula $(Bi_2O_2)^{2+}(A_{m-1}B_mO_{3m+1})^{2-}$ where A is Bi^{3+}, Ba^{2+}, Sr^{2+}, Ca^{2+}, Pb^{2+}, K^+ or Na^+, while B is Ti^{4+}, Zr^{4+}, Nb^{5+}, Ta^{5+}, Mo^{6+}, W^{6+} or Fe^{3+} [2,3]. With regard to applications as NVFRAM, $SrBi_2Nb_2O_9$ (SBN) and $SrBi_2Ta_2O_9$ (SBT) (and quite recently also $(Bi,La)_4Ti_3O_{12}$ (BLT) [4]) are the most important among the members of the Aurivillius family, with A: Sr^{2+} and B: Ta^{5+} or Nb^{5+} ($m = 2$).

SBN and SBT thin films or bulk powders have been prepared following various synthesis routes like metalorganic

* Corresponding author. Tel.: +32 11 26 8308; fax: +32 11 26 8301.
E-mail address: jules.mullens@luc.ac.be (J. Mullens).

0040-6031/$ – see front matter © 2004 Elsevier B.V. All rights reserved.
doi:10.1016/j.tca.2004.07.005

decomposition (MOD) [5], pulsed laser ablation deposition (PLD) [6–8], metalorganic chemical vapor deposition (MOCVD) [9], polymeric precursor route [10] and alcoholic sol–gel [11,12].

The phase formation temperature, chemical homogeneity, phase purity and electrical properties of multicomponent electroceramic materials like SBN and SBT are highly dependent on the cation homogeneity in the oxide precursor [13]. In this respect the chemical preparation routes, like the sol(ution)–gel synthesis, are extremely useful. These methods allow for the synthesis of precursors, in which the constituent metal ions are mixed on an atomic scale, leading to lower processing temperatures, shorter sintering times (low thermal budget) and more homogeneous end products. Moreover, the stoichiometry is easy to control and it is possible to prepare thin films using simple coating techniques like spin- and dipcoating.

In this study, an aqueous solution–gel route was applied for the synthesis of SBN. Starting from rather inexpensive, easily available salts 'dissolved' in water, this method offers a low-cost and environmentally friendly alternative to the conventional sol–gel techniques using organic solvents and metal alkoxides. An additional advantage is the insensitivity of the reagents towards air and humidity. This method has turned out to be an interesting approach for the synthesis of several electroceramic materials (both powders and thin films) [14–18].

Once the amorphous precursor gel (maintaining the homogeneous mixing of the constituent metal ions) is prepared, the desired oxide phase can be obtained by an appropriate heat treatment. An important issue during the decomposition and phase formation is the conservation of the homogeneous cation distribution. Moreover, since the electrical properties of the final oxide film seem to be heavily dependent upon the applied heat treatment [19], detailed knowledge about the precursor's behaviour during thermal treatment is of paramount importance. For these reasons, the thermal decomposition of the SBN gel was extensively studied using thermoanalytical techniques. Additionally, the precursor homogeneity was evaluated using electron microscopy and room temperature X-ray diffraction (XRD), while crystallization was studied by high temperature X-ray diffraction (HT-XRD).

2. Experimental

2.1. Materials and reagents

For the gel synthesis the following materials and reagents were used: citric acid (Aldrich, 99%, C(OH)(COOH)$(CH_2COOH)_2$), ammonia (UCB, p.a. NH_3 ca. 25% in H_2O), niobium(V) ammonium oxalate (H.C. Starck, 20.7% in Nb), hydrogen peroxide (Acros Organics, 35 wt.% solution in water, stabilized, H_2O_2), strontium acetate (Aldrich, 99.995%, $Sr(CH_3COO)_2$), bismuth acetate (Aldrich, 99.99+ %, $Bi(CH_3COO)_3$) and acetic acid (UCB, 99–100%, p.a., 1.049 kg/L, CH_3COOH).

2.2. Aqueous solution–gel synthesis of the SBN acetate–citrate gel

To start with, the aqueous solution–gel synthesis of multimetal oxides requires the preparation of a stable, clear and homogeneous precursor solution containing the different metal ions. Moreover, upon solvent evaporation this solution must be converted into an amorphous gel maintaining the homogeneity on atomic scale. A flowchart of SBN gel synthesis is shown in Fig. 1. A 0.2 mol/L Nb-precursor was synthesized as described elsewhere [20], by dissolution of niobium (V) ammonium oxalate in an aqueous solution of citric acid and hydrogen peroxide (the oxalate is decomposed by reaction with H_2O_2). A 0.05 mol/L aqueous bismuth precursor solution was prepared by dissolving bismuth acetate in glacial acetic acid, followed by dilution with water. In order to obtain a stable solution, an amount of 8 mL CH_3COOH was necessary to dissolve 1 g Bi-acetate. A strontium acetate solution (0.2 mol/L) was synthesized by dissolving strontium acetate in water. The exact precursor metal concentrations were measured by means of ICP-AES, using a Perkin-Elmer Optima 3000 DV.

The trimetallic SBN precursor solution was obtained by mixing the monometallic solutions in stoichiometric amounts. In order to prevent precipitation (of Sr and Bi), an excess of citric acid had to be added until the citric acid: metal ion molar ratio was equal to 3:1 and the pH had to be increased by the addition of ammonia until 4.5. The as-synthesized precursor solution was poured out in a petri vessel and the solvent was evaporated in a furnace at 100 °C under flowing air. The resulting gel was colourless, transparent and amorphous, as was shown by XRD. The gel was however rather hygroscopic and hence sticky. In order to allow the gel to be removed from the petri vessel, it needed a further heating step at 150 °C.

2.3. Characterization techniques

The thermal decomposition pathway of the SBN precursor gel was studied using complementary thermoanalytical techniques. Thermogravimetric analysis–evolved gas analysis (TGA–EGA) allowed for the measurement of the weight loss and the analysis/identification of the gases released during heating [21]. TGA–FTIR experiments were carried out on a TGA 951-2000 apparatus from TA instruments, on-line coupled to a Bruker IFS 48 FTIR-spectrometer. On-line TGA–MS measurements were done by coupling the TGA apparatus to a quadrupole thermolab VG fisons instruments mass spectrometer, using a flexible heated silica lined steel capillary and a molecular leak. The evolving gas molecules are fragmented during ionization. In order to be able to distinguish between NH_3^+ and OH^+, both at *m*/*z* 17, all measurements were carried out at an ionization energy of 20 eV

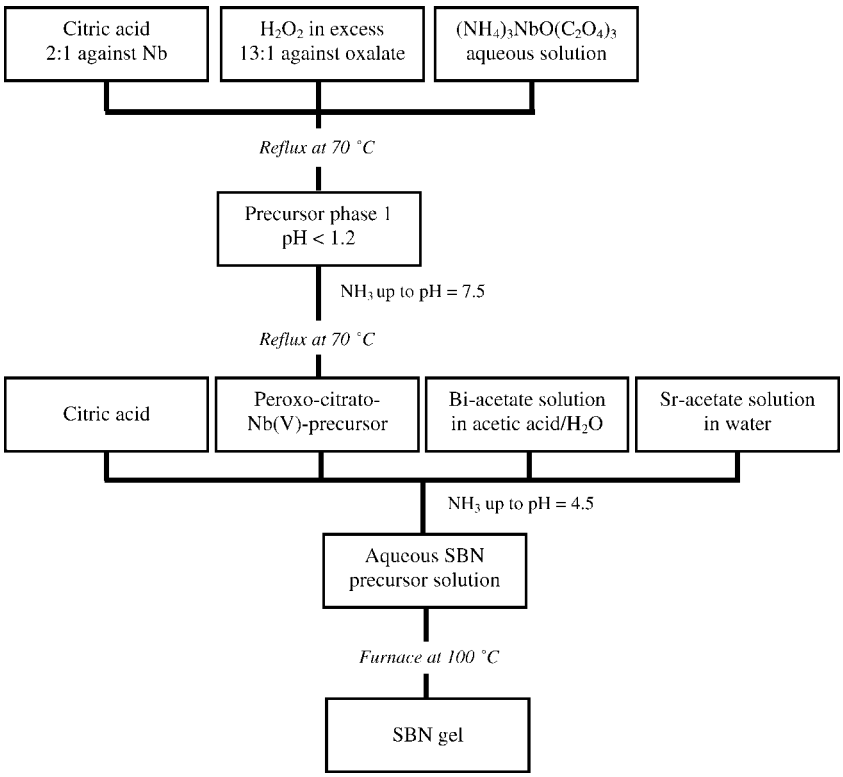

Fig. 1. Flowchart for the synthesis of the strontium bismuth niobate precursor gel.

instead of 70 eV, which is usually applied, since at low energy the creation of OH^+-ions is inhibited [22].

Complementary to TGA–MS and TGA–FTIR, the changes in the solid state of the gel during thermal decomposition were studied using high temperature diffuse reflectance infrared fourier transform spectroscopy (HT-DRIFT). These measurements were done on a Bruker IFS 66 spectrometer equipped with a high temperature-high pressure chamber with parabolic ZnSe windows (Spectratech Inc.). The HT-DRIFT investigations were performed on 2 (w/w%) samples in KBr. Measurements in dry air are only possible up to 400 °C, since at higher temperature the equipment would be damaged. In order to study the decomposition at higher temperature, the SBN gel was heated in dry air in a TGA furnace up to the desired temperature. Afterwards the DRIFT-spectra of the resulting powders were recorded at room temperature (off-line).

For all the TGA–MS, TGA–FTIR and HT-DRIFT measurements, a heating rate of 10 °C/min and a gas flow rate of 100 mL/min were applied (dry air, He or Ar).

The homogeneity of the precursor throughout the entire thermo-oxidative decomposition was evaluated by TEM measurements on freestanding thin films and by SEM measurements on powders. The films were prepared by dotting a droplet of the precursor solution onto a gold TEM grid, subsequently heating it in a quartz tube furnace in flowing dry air (100 mL/min) at a heating rate of 10 °C/min up to the desired temperature and finally quenching it. TEM studies were done on a Philips CM12 at 120 kV and SEM experiments were carried out on a Philips XL30 FEG-SEM. Both electron microscopes are equipped with an energy dispersive X-ray detector (EDX) and a super ultra thin window.

Transformation of the amorphous precursor gel into the crystalline phase(s) during heating was evaluated by means of HT-XRD. High temperature X-ray diffraction patterns were recorded on a Siemens D5000 diffractometer equipped with a Göbel mirror (Cu Kα1, Huber), a high temperature sample stage (Anton Paar, HTK10) and a position sensitive detector (mBraun). The Pt rod of the heating stage also contributes to the diffraction pattern with peaks at 39.76, 46.24 and 67.45° 2θ. The precursor gel was heated at 10 °C/min in static air to the desired temperature and after a 30 s delay time an entire XRD pattern was measured within approximately 9 min.

3. Results and discussion

3.1. Thermal decomposition

Fig. 2 shows the HT-DRIFT spectra of the SBN gel during heating at 10 °C/min in dry air. The spectrum at 100 °C offers information about the structure of the gel network and about the constituent metal complexes. It is our belief that gel formation is not only a consequence of the increase in concentration and viscosity upon solvent evaporation. The formation of intermolecular crosslinks like ammonium-carboxylate interactions and hydrogen bonds is also assumed to be a key factor for obtaining a homogeneous and stable

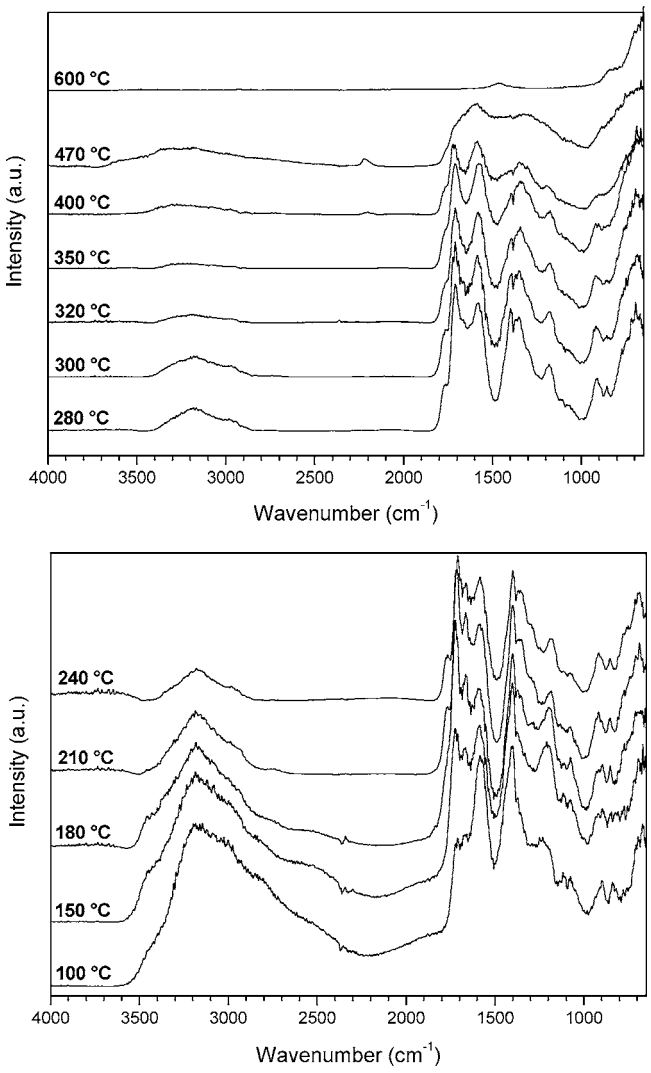

Fig. 2. HT-DRIFT spectra of the SBN gel in dry air (10 °C/min, 100 mL/min).

gel [23]. The two prominent peaks in the DRIFT-spectrum at 100 °C at 1575 and 1400 cm^{-1} are ascribed to the asymmetric ($\nu_{as}(COO^-/NH_4^+)$ and/or $\nu_{as}(COO^-/M^{n+})$) and symmetric ($\nu_{sym}(COO^-/NH_4^+)$ and/or $\nu_{sym}(COO^-/M^{n+})$) stretch of the carboxylate functions, respectively. The hydrogen bonded ν(OH) and ν(NH) stretches can be distinguished in a broad band between 3500 and 2500 cm^{-1}. The existence of (peroxo-)citrato metal complexes is confirmed by the following vibrations in the spectrum at 100 °C: the C–O stretch of the α-hydroxy group of citric acid coordinated to the metal ion ($\nu(C–O)_{CO\text{-}metal}$) can be observed around 1080 and at 855 cm^{-1} the $\nu_1(Nb < O_2)$ stretch of the side-on bonded peroxo-groups in the peroxo-citrato-Nb-precursor, used for the synthesis of the SBN gel, is situated [24].

In Figs. 3 and 4 the TGA and DTG profiles of the thermal decomposition of the SBN gel in dry air and inert atmosphere, respectively are shown. The thermal decomposition behaviour in dry air can be divided in four temperature regions: 25–120 °C, 120–270 °C, 270–450 °C and above

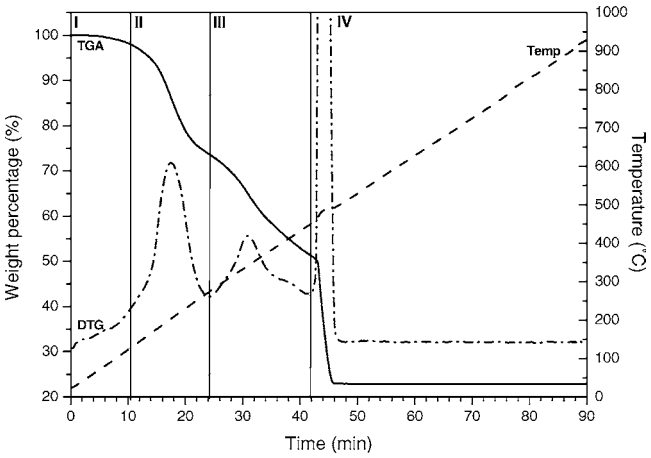

Fig. 3. TGA/DTG profile of the SBN gel in dry air (10 °C/min, 100 mL/min), divided in four temperature regions (I–IV).

450 °C. The first three steps of the profile in dry air are also distinguishable in inert atmosphere. However, the large weight loss around 475 °C in dry air is not measured in inert atmosphere, instead an additional loss is observed at higher temperature (above 700 °C). The reactions taking place at higher temperature correspond to the gradual decomposition of the residual organic matter due to the lack of oxygen. More information about the reactions taking place during thermal decomposition of the SBN gel is obtained from the complementary HT-DRIFT and TGA–EGA (TGA–MS and TGA–FTIR) experiments.

When the gel is heated, water is evaporated at about 100 °C as illustrated by the evolution of *m/z* 18 in TGA–MS in dry air and in helium (Fig. 5 and Fig. 6). This release is responsible for the first weight loss in the TGA profiles and can be explained by the hygroscopic character of the precursor gel (drying of the gel).

In the second temperature region the organic gel matrix is partly decomposed, whereas the direct coordination of the metal ions remains intact. The HT-DRIFT spectra at 180 and

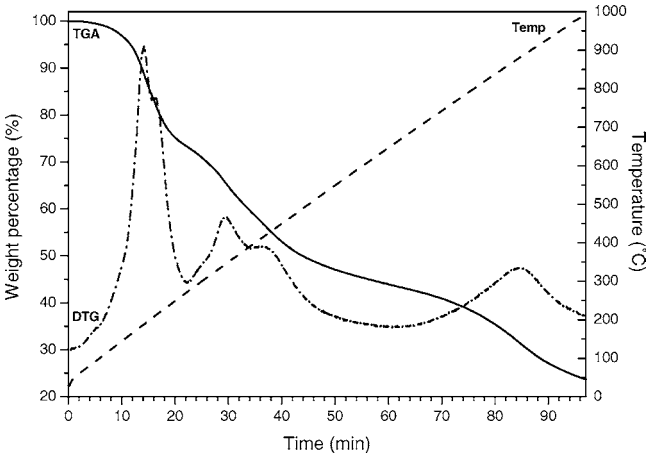

Fig. 4. TGA/DTG profile of the SBN gel in inert atmosphere (argon, helium) (10 °C/min, 100 mL/min).

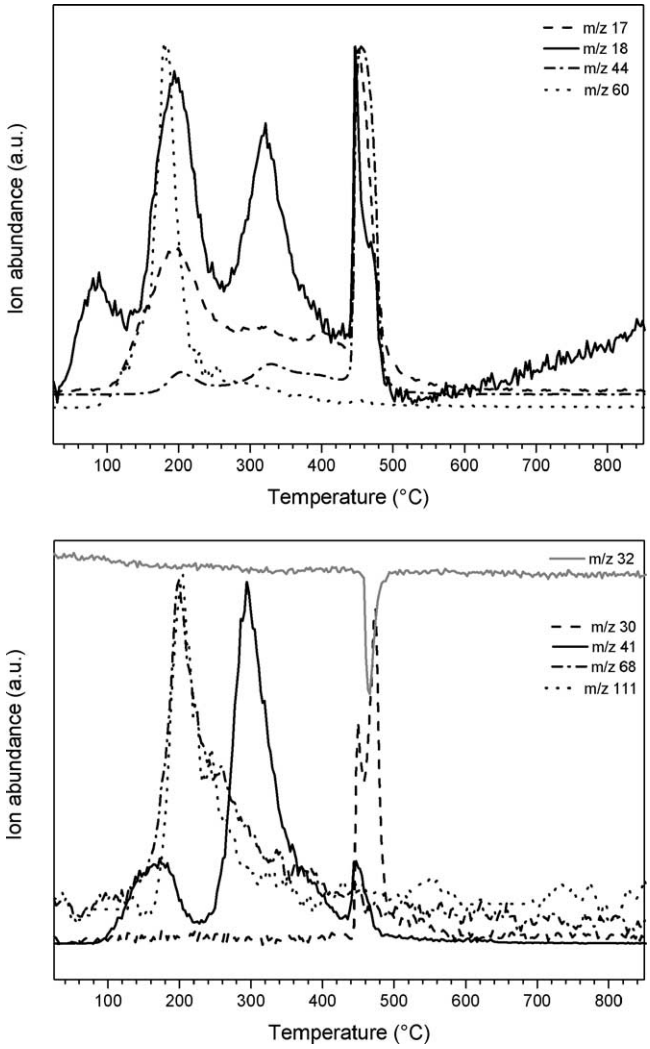

Fig. 5. TGA–MS profiles of the SBN gel in dry air (10 °C/min, 100 mL/min).

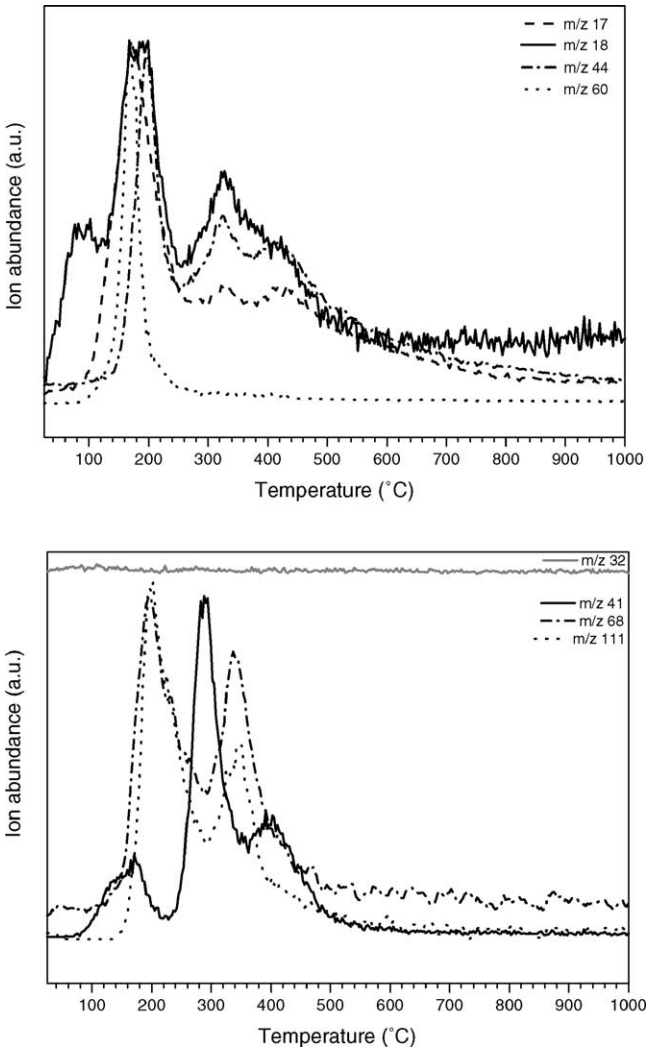

Fig. 6. TGA–MS profiles of the SBN gel in helium (10 °C/min, 100 mL/min).

210 °C (Fig. 2) illustrate the decrease of the intensities of the bands at 1575 and 1400 cm^{-1}, while the absorption at 1720 cm^{-1} due to the C=O stretch of free carboxylic acid functions becomes stronger. At the same temperatures, the evolution of ammonia is observed (Figs. 5 and 6 TGA–MS, evolution of *m*/*z* 17 and Figs. 7 and 8 TGA–FTIR, wavenumber interval 940–913 cm^{-1}) as well as acetic acid (*m*/*z* 60 in MS and wavenumber interval 1840–1730 cm^{-1} in FTIR). All these features indicate the typical decomposition of ammonium citrate and ammonium acetate present in the gel precursor. An important feature is that it seems that all the acetic acid has evolved below 250 °C. This is important because it gives evidence for the fact that the acetate groups are not or only very weakly coordinated to the metal ions. Note that this is different compared to other aqueous acetate–citrate precursors, as for example a zinc acetate–citrate precursor gel [25].

Around 200 °C TGA–MS shows the release of H_2O (*m*/*z* 18), $C_3H_3^+$ (*m*/*z* 39) and $C_4H_4O^+$ (*m*/*z* 68). These mass fragments indicate the decomposition of the free citric acid

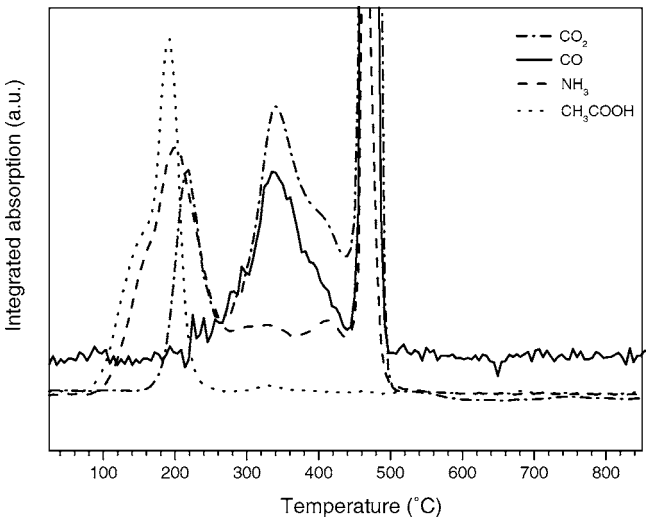

Fig. 7. TGA–FTIR profiles of the SBN gel in dry air (10 °C/min, 100 mL/min).

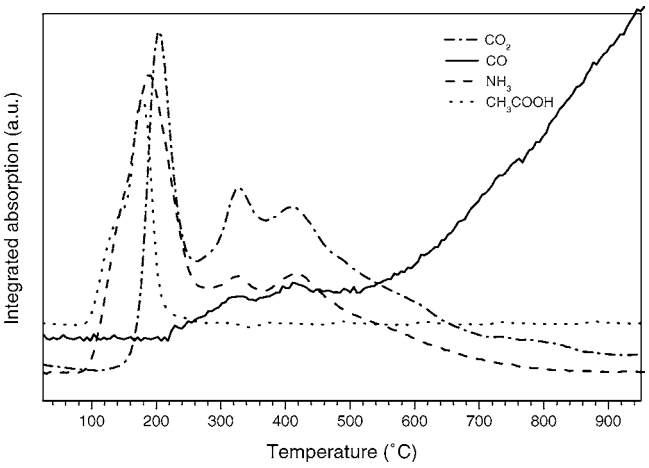

Fig. 8. TGA–FTIR profiles of the SBN gel in argon (10 °C/min, 100 mL/min).

(formed out of ammonium citrate at lower temperature) into unsaturated carboxylates/carboxylic acids and anhydrides [17]. According to Rajendran et al. [26] and Van Werde et al. [25] citric acid decomposes at low heating rate via a series of endothermic dehydroxylation and decarboxylation steps with formation of aconitic acid, itaconic acid, itaconic anhydride and citraconic anhydride successively. The absorption at 1780 cm^{-1} in the HT-DRIFT spectrum recorded at 210 °C clearly illustrates this anhydride formation in the solid state. At high magnification an absorption peak at 1840 cm^{-1} is observed in the spectrum at 180 °C, which can also be ascribed to the formation of anhydrides in the solid state.

In the same temperature region also the release of CO_2 is observed (*m*/*z* 44 in MS and wavenumber interval 2395–2220 cm^{-1} in FTIR). Since this evolution also occurs in inert atmosphere (see Figs. 6 and 8), it is concluded that the CO_2 release is due to the decarboxylation reactions of the remaining unsaturated carboxylic acids and not a result of combustion reactions.

The TGA–MS experiments also confirm the formation and evaporation of amides and imides out of the ammonium carboxylates present in the gel. For both oxidizing and inert conditions it is possible to detect the evolution of the fragment with *m*/*z* 111, corresponding with 3-methyl-maleimide ($C_5H_5NO_2^+$). This is a cyclic imide that can be formed by a nucleophilic attack of ammonia on an acid group, leading to the formation of an amide. 3-methyl-maleimide is formed by a subsequent intramolecular dehydration, followed by an isomerization [27].

A second indication for the formation of amides is the release in dry air and in inert atmosphere of a fragment with *m*/*z* 41, which refers to $NH{=}C{=}CH_2^+$. This is a typical ion fragment formed by a McLafferty rearrangement after ionization of an aliphatic nitrile containing a γ-hydrogen (the latter formed out of an amide by dehydration) [27]. Although the maximum of the *m*/*z* 41 profile is situated around 300 °C (thus in the third temperature region), it can already be detected at lower temperatures.

In the third temperature region the direct coordination sphere of the metal ions is decomposed. Around 300 °C the dehydroxylation of the metal-complexes takes place (breakdown of the α-hydroxy-coordination of the metal ion). This is obvious from the disappearance of the $\nu(C{-}O)_{CO\text{-metal}}$ stretch at 1080 cm^{-1} between 280 and 320 °C in the HT-DRIFT spectra (Fig. 2). From the HT-DRIFT spectra it is also clear that the side-on peroxo-groups are decomposed between 320 and 350 °C by the disappearance of the absorption at 855 cm^{-1}. From these two observations it can be concluded that the (peroxo-)citrato metal complexes are decomposed. TGA–EGA also shows the release of CO_2, in dry air as well as in inert atmosphere, as a consequence of the decarboxylation of the remaining carboxylic acids. In dry air the CO_2 release is however more pronounced compared to the decomposition in inert conditions. Moreover, when comparing the TGA profiles in dry air and inert atmosphere it is obvious that about 5% more weight is lost during the third step in the presence of oxygen (see Figs. 3 and 4). This can possibly be explained by the oxidative combustion of some organic compounds in dry air. The decomposition of the metal ion carboxylates is confirmed by the decreased absorption intensity for the metal carboxylate stretches ($\nu_{as}(COO^-/M^{n+})$ at 1575 cm^{-1} and $\nu_{sym}(COO^-/M^{n+})$ at 1400 cm^{-1}) when comparing the spectra at 320 °C and 400 °C in HT-DRIFT. As mentioned before, the release of *m*/*z* 41 is observed in the same temperature region in TGA–MS, which can be ascribed to aliphatic nitriles. The formation of these nitriles in the gel is confirmed by the absorption at 2200 cm^{-1} in the HT-DRIFT spectrum at 400 °C.

During the fourth step the residual organic compounds are decomposed oxidatively in dry air. In a temperature interval of about 50 degrees the highly exothermal decomposition causes a rapid weight loss of ±25%. The increase in temperature (see Fig. 3, temperature profile) indicates the ignition of the sample. The consumption of oxygen in this region is illustrated by the decrease of the signal at *m*/*z* 32 (O_2^+) in TGA–MS, ascribed to the drop of the oxygen pressure in the TGA furnace and as a consequence in the mass spectrometer. TGA–MS and TGA–FTIR show the release of NH_3, NO, CO and nitriles, indicating the incomplete oxidation due to the temporary drop in oxygen pressure. More ordinary combustion products like CO_2, H_2O and NO_2 are also detected. The HT-DRIFT spectra at 470 and 600 °C confirm these combustion reactions by a decrease of the absorption of the corresponding functional groups in the wavenumber region 2000–1000 cm^{-1}.

When looking at the decomposition in inert conditions, it is clear that due to the absence of oxygen the citrate ligands are not burnt away instantly after their decoordination from the metal ions. Instead, a gradual decomposition of the residual organic matter takes place, which is not yet completed at 1000 °C as indicated by the TGA profile (Fig. 4) and the CO signal in TGA–FTIR (Fig. 8). Obviously the perovskite SBN phase has not formed. The XRD pattern (not shown) of the powder obtained by heating the precursor up

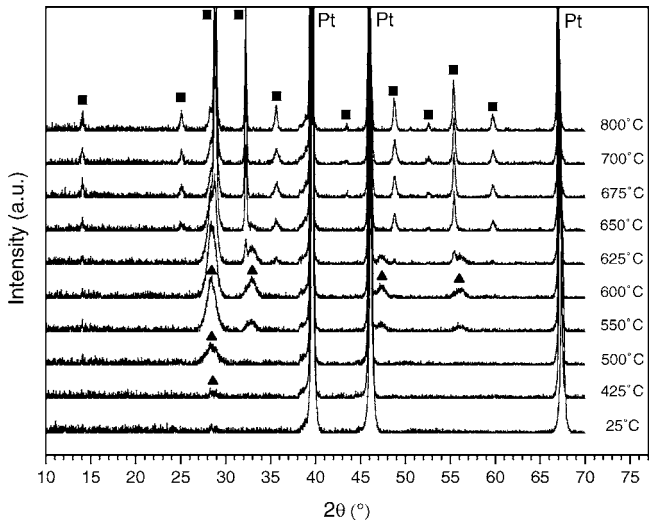

Fig. 9. HT-XRD patterns of the $SrBi_2Nb_2O_9$ precursor, heated at 10 °C/min in static air (■: perovskite–SBN and ▲: fluorite–SBN).

to 1000 °C in helium, shows the presence of a small amount of metallic Bi.

3.2. Phase formation

In order to study the phase formation of $SrBi_2Nb_2O_9$, the decomposition and crystallization of the precursor was in-situ followed during a HT-XRD experiment. As can be observed from Fig. 9, diffuse patterns are recorded for the gel heated up to 400 °C, indicating the precursor to be amorphous up to that temperature. At 425 °C the intermediate fluorite phase starts to form, which is in excellent agreement with the TEM experiments described in paragraph 3.3 and with the thermo-analytical experiments reported in paragraph 3.1. The latter showed that the coordination of the metal ions is changed during the third temperature region, at a temperature below 400 °C. The XRD measurements illustrate that immediately hereafter the crystallization starts. These observations also imply that oxide formation already starts before the final decomposition step of the precursor gel (see Fig. 3, around 475 °C). An analogous result was obtained by Mondelaers et al. [18] and Van Werde et al. [25] for a Zn–acetate–citrate precursor.

The fluorite phase starts to convert into the desired ferroelectric perovskite phase at 625 °C. At 675 °C only perovskite SBN can be observed, indicating that all fluorite has been converted. At higher temperatures the diffraction peaks become more intense due to crystallite growth. No secondary phases are detected at any temperature.

One of the main problems, related to the integration of SBN and SBT materials in nonvolatile memories, is the high processing temperature [28]. Temperatures above 700 °C are needed to obtain crystalline films without secondary non-ferroelectric phases. These temperatures are not compatible with the VLSI fabrication techniques. Therefore a lot of research has been carried out in order to lower the crystallization temperature. It has been shown that the addition of an excess of Bi^{3+} is one possibility to achieve this, since this would have the effect of promoting the crystallization from fluorite phase to the Bi-layered structure and enhancing the grain growth [29,30]. In order to study the influence of excess Bi^{3+} on the crystallization behaviour of our aqueous precursor, precursors were prepared with 10% ($SrBi_{2.2}Nb_2O_{9\pm y}$) and 20% of Bi-excess ($SrBi_{2.4}Nb_2O_{9\pm y}$), following the flowchart in Fig. 1. Afterwards a HT-XRD experiment was done on the resulting gels (patterns not shown). For both samples the intermediate fluorite phase is formed, which is transformed into the desired perovskite phase on further heating, analogous to the stoichiometric sample. No secondary phases can be observed (e.g. Bi-oxide), indicating bismuth is not segregated but incorporated in the SBN crystal structure. This is important with regard to the preparation of ferroelectric thin films, since the formation of the highly conductive Bi_2O_3 secondary phase would lead to a high leakage current and poor hysteresis properties [31]. Note that this result differs from that obtained for an analogous aqueous $(Bi,La)_4Ti_3O_{12}$ (BLT) precursor, for which at higher temperatures the Bi^{3+}-excess leads to the formation of a bismuth oxide secondary phase [32]. Further details about precursor homogeneity are reported in paragraph 3.3.

An important issue is however that the temperature, at which the transformation of the fluorite phase into the perovskite phase takes place, appears to be lower when the Bi-content is higher. This is illustrated in Fig. 10, showing the XRD-patterns of the three different precursors heated up to 625 °C: the ratio of perovskite phase to fluorite phase (ratio of integrated peak intensities) is higher for the samples with Bi-excess compared to the stoichiometric sample. These results illustrate the possibility of lowering the crystallization temperature of the perovskite phase (out of the intermediate fluorite phase) by the addition of an excess of bismuth to the aqueous precursor solution. This is an interesting conclusion with regard to the preparation of

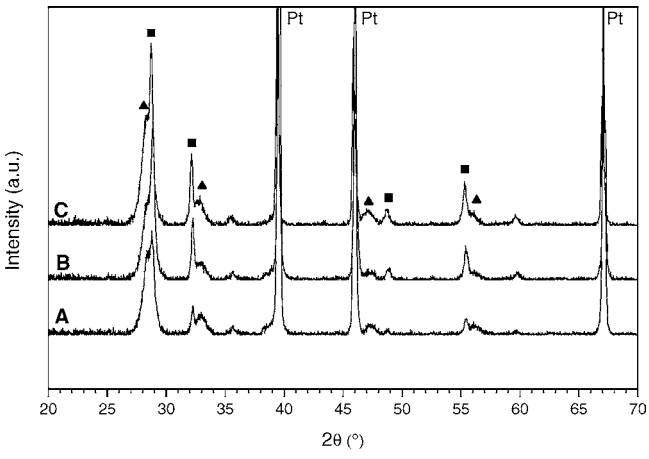

Fig. 10. HT-XRD patterns at 625 °C for $SrBi_{2.0}Nb_2O_9$ (A), $SrBi_{2.2}Nb_2O_{9\pm y}$ (B) and $SrBi_{2.4}Nb_2O_{9\pm y}$ (C) (■: perovskite–SBN and ▲: fluorite–SBN).

ferroelectric thin films for application as nonvolatile memory at low temperature.

3.3. Precursor homogeneity

To enable the crystallization of the desired oxide phase out of the precursor gel, obtaining a homogeneous cation distribution just prior to oxide formation is as important as synthesizing a homogeneous gel [23]. Based on the HT-XRD results described above, one might conclude the precursor to be homogeneous during the entire thermal decomposition, since no diffraction peaks of secondary phases are measured at any time during thermal treatment. However, this conclusion is in some way premature. In spite of the great advantage of measuring XRD-patterns in situ during heating, the HT-XRD technique has one important disadvantage. Since patterns are recorded at high temperatures, it is not possible to measure molten secondary phases. For example, a previous SBN citrate-ethylenediamine precursor [20] showed metallic Bi segregation at 400 °C, which could not be detected with HT-XRD since bismuth melts at 271.40 °C [33]. Therefore, in this work the precursor homogeneity was evaluated using TEM, SEM and room temperature XRD.

At first the homogeneity of the precursor was evaluated for powders. In order to check this, both the $SrBi_2Nb_2O_9$ and $SrBi_{2.4}Nb_2O_{9\pm y}$ precursor gels were heated in dry air up to 400 °C and then quenched. The resulting powders were characterized using SEM and XRD (Fig. 11). In case of the stoichiometric sample no phase segregation is detected, the sample is totally homogeneous. The XRD diffraction peak between 2θ equal to 25 and 30° can be ascribed to the fluorite phase. On the contrary, the SEM micrograph (white particles in the SEM–BSE image) and the XRD pattern of the powder with Bi-excess show a small fraction of metallic Bi segregation. A possible explanation is the lack of oxygen during thermal decomposition. As a consequence Bi^{3+} is reduced to Bi. Upon further heating this Bi is oxidized again to Bi^{3+} and incorporated in the $SrBi_2Nb_2O_9$ perovskite structure [20].

However, since the inhomogeneity observed in this way is ascribed to a bulk effect (namely the lack of available oxygen, resulting in reducing conditions during thermal decomposition) and for most of the applications SBN is processed as thin film, it was considered important to also investigate the homogeneity during thermal decomposition of a (freestanding) thin film of the SBN precursor. For, inhomogeneity of the precursor as (bulk) powder does not automatically imply its inhomogeneity as a (freestanding) thin film, since the ratio between available oxygen and precursor quantity during thermal decomposition is much higher in the case of thin films. In order to check this, TEM experiments were carried out on freestanding thin films. At first, our attention was focused on the temperature region around the final decomposition step of the stoichiometric $SrBi_2Nb_2O_9$ precursor. Two films were prepared: the first was heated up to 460 °C (just before the final decomposition step) and afterwards quenched, the other one was heated up to 550 °C (just after the final step), kept isothermal at this temperature for 10 minutes and finally quenched. Bright field (BF) images, dark field (DF) images and diffraction patterns were measured for both films. The film at 460 °C is predominantly amorphous and homogeneous, however, already some very small grains with an average size less than 5 nm can be detected, as illustrated in Fig. 12A. The HT-XRD experiment (see paragraph 3.2 and Fig. 9) indeed showed that the intermediate fluorite SBN phase has already started to form at this temperature. Crystallinity is however poor, as illustrated by the diffraction pattern. At 550 °C (Fig. 12B) the BF image shows the 'puffed up' morphology as a consequence of the evolution of volatile reaction products [32]. It is evident that the sample contains a (nano)crystalline phase: the diffraction pattern shows several rings and in DF some crystallites do light up.

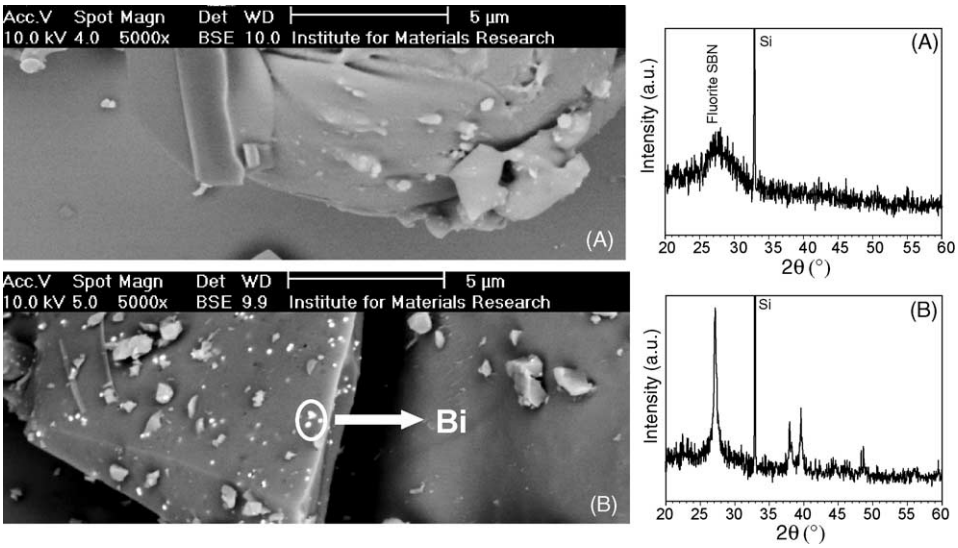

Fig. 11. SEM micrograph and room temperature XRD pattern of the SBN gel, heated up to 400 °C in dry air with (A) $SrBi_{2.0}Nb_2O_9$ and (B) $SrBi_{2.4}Nb_2O_{9\pm y}$.

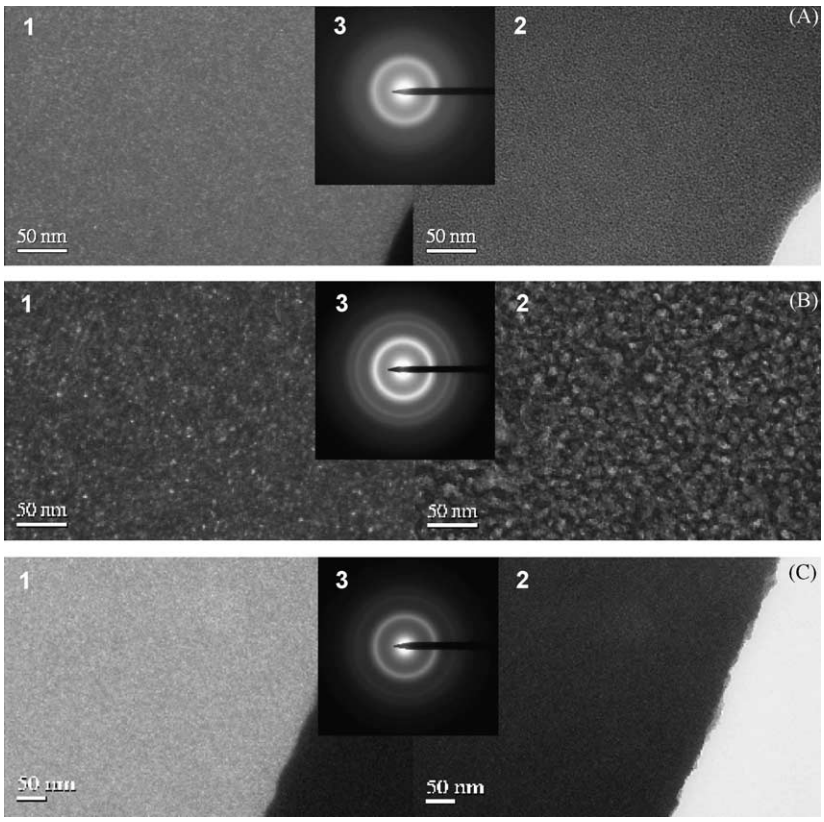

Fig. 12. TEM micrographs of freestanding thin films of the SBN precursor: (1) DF image, (2) BF image and (3) diffraction pattern with (A) $SrBi_{2.0}Nb_2O_9$ precursor at 460 °C, (B) $SrBi_{2.0}Nb_2O_9$ precursor at 550 °C (during 10 min) and (C) $SrBi_{2.4}Nb_2O_{9\pm y}$ precursor at 400 °C.

In order to study the influence of the Bi-excess on precursor homogeneity, a freestanding thin film of the solution with 20% of Bi-excess ($SrBi_{2.4}Nb_2O_{9\pm y}$) was heated up in dry air to 400 °C, since the powder showed Bi-segregation at this temperature. However, for the thin film the TEM-micrographs (Fig. 12C) again illustrate the homogeneity of the precursor at this temperature, similar to the stoichiometric sample. Metallic Bi cannot be detected.

These experiments illustrate that the gel formed by evaporation of the SBN precursor solution as a thin film is homogeneous and, moreover, its homogeneity is maintained during the entire thermo-oxidative decomposition until crystallization starts. These results show the difference in crystallization behaviour between powders and (freestanding) thin films.

4. Conclusion

The thermal decomposition behaviour of a $SrBi_2Nb_2O_9$ acetate–citrate precursor, prepared by the aqueous solution–gel method, was unraveled by a combination of complementary thermoanalytical techniques. In dry air, four regions can be distinguished. In the first two regions the gel matrix is decomposed, leaving the metal ion coordination intact. The third step on the other hand comprises the decomposition of the metal ion complexes, as indicated by the breakdown of the peroxo- and the α-hydroxy-coordination of the metal ions. The last step is characterized by the oxidative combustion of the organic residue. The decomposition in inert atmosphere runs parallel with the one in dry air at temperatures until approximately 350 °C. However, at higher temperatures the oxidative decomposition is replaced by a gradual decomposition, due to the lack of oxygen, which is not yet completed at a temperature of 1000 °C.

Precursor homogeneity during thermal treatment was evaluated on freestanding thin films using TEM and on powder samples using SEM and room temperature XRD. The stoichiometric precursor ($SrBi_2Nb_2O_9$) turns out to be homogeneous during the entire thermo-oxidative decomposition, in case of the thin film as well as the powder. The Bi^{3+}-excess precursor ($SrBi_{2.4}Nb_2O_{9\pm y}$) on the other hand shows metallic Bi-segregation in powder form, while the freestanding thin film is homogeneous, probably because of the lack of oxygen during thermal decomposition in case of the powder sample. On further heating this Bi is oxidized again and incorporated in the SBN perovskite structure.

High temperature X-ray diffraction experiments illustrated that the intermediate fluorite phase is formed out of the amorphous precursor gel at about 425 °C, immediately after the ‘release’ of the metal ions from the organic network as shown by the thermal analysis. The onset temperature for transformation into the ferroelectric perovskite phase is dependent upon the Bi^{3+}-content: the Bi^{3+}-excess sample shows a higher perovskite to fluorite ratio at 625 °C

compared to the stoichiometric sample. An interesting observation is that the excess of Bi^{3+} does not lead to the formation of the Bi_2O_3 secondary phase, which is extremely important for the thin film ferroelectric properties in a later stadium. This indicates that the processing temperature of SBN (and SBT) can be lowered by changing the metal ion ratio of the precursor solution, which is extremely important with regard to the preparation of thin films for NVFRAM applications.

Recently we managed to deposit thin films by aqueous chemical solution deposition (CSD) [15,34]. Future work will be focused on optimizing the heat treatment of the as-deposited amorphous thin films in order to obtain good ferroelectric properties. In this regard the results described in this work concerning thermal decomposition, precursor homogeneity and phase formation are of great importance.

Acknowledgements

D. Nelis and A. Hardy are research assistants and M.K. Van Bael and G. Vanhoyland are postdoctoral fellows of the Fund for Scientific Research Flanders, Belgium (FWO-Vlaanderen). This research is partially financed by ‘Het Vlaamse Gewest - IWT’.

References

[1] C.A. Paz de Araujo, J.D. Cuchiaro, L.D. McMillan, M.C. Scott, J.F. Scott, Nature 374 (1995) 627–629.
[2] B. Aurivillius, Arkiv for Kemi 1 (1949) 463–480.
[3] E.C. Subbarao, Integr. Ferroelectr. 12 (1996) 33–41.
[4] B.H. Park, B.S. Kang, S.D. Bu, T.W. Noh, J. Lee, W. Jo, Nature 401 (1999) 682–684.
[5] S.B. Desu, T. Li, Mater. Sci. Eng. B 34 (1995) L4–L8.
[6] A. Pignolet, K.M. Satyalakshmi, M. Alexe, N.D. Zakharov, C. Harnagea, S. Senz, D. Hesse, U. Gösele, Integr. Ferroelectr. 26 (1999) 21–29.
[7] S.B. Desu, D.P. Vijay, X. Zhang, B. He, Appl. Phys. Lett. 69 (12) (1996) 1719–1721.
[8] J. Lettieri, M.A. Zurbuchen, Y. Jia, D.G. Schlom, S.K. Streiffer, M.E. Hawley, Appl. Phys. Lett. 76 (20) (2000) 2937–2939.
[9] T. Li, Y. Zhu, S.B. Desu, C.-H. Peng, M. Nagata, Appl. Phys. Lett. 68 (5) (1996) 616–618.
[10] S.M. Zanetti, E.R. Leite, E. Longo, J.A. Varela, J. Eur. Ceram. Soc. 19 (1999) 1409–1412.
[11] A. Gonzalez, R. Jimenez, J. Mendiola, M.L. Calzada, Integr. Ferroelectr. 30 (2000) 281–289.
[12] M.A. Rodriguez, T.J. Boyle, B.A. Hernandez, C.D. Bucheit, M.O. Eatough, J. Mater. Res. 11 (9) (1996) 2282–2287.
[13] M. Kakihana, J. Sol–Gel Sci. Technol. 6 (1996) 7–55.
[14] D. Nelis, K. Van Werde, D. Mondelaers, G. Vanhoyland, M.K. Van Bael, J. Mullens, L.C. Van Poucke, J. Eur. Ceram. Soc. 21 (2001) 2047–2049.
[15] D. Nelis, M.K. Van Bael, H. Van den Rul, J. Mullens, L.C. Van Poucke, G. Vanhoyland, J. D’Haen, W. Laureyn, D.J. Wouters, Integr. Ferroelectr. 45 (2002) 205–213.
[16] K. Van Werde, G. Vanhoyland, D. Nelis, D. Mondelaers, M.K. Van Bael, J. Mullens, L.C. Van Poucke, J. Mater. Chem. 11 (2001) 1192–1197.
[17] A. Hardy, K. Van Werde, G. Vanhoyland, M.K. Van Bael, J. Mullens, L.C. Van Poucke, Thermochim. Acta 397 (2003) 143–153.
[18] D. Mondelaers, G. Vanhoyland, H. Van den Rul, J. D’Haen, M.K. Van Bael, J. Mullens, L.C. Van Poucke, Mater. Res. Bull. 37 (5) (2002) 901–914.
[19] D. Nelis, D. Mondelaers, G. Vanhoyland, H. Van den Rul, M.K. Van Bael, J. Mullens, L.C. Van Poucke, J. D’Haen, D.J. Wouters, Integr. Ferroelectr., in press.
[20] D. Nelis, K. Van Werde, D. Mondelaers, G. Vanhoyland, H. Van den Rul, M.K. Van Bael, J. Mullens, L.C. Van Poucke, J. Sol–Gel Sci. Technol. 26 (1-3) (2002) 1125–1129.
[21] J. Mullens, Evolved Gas Analysis, in: P.K. Gallagher, M.E. Brown (Eds.), Handbook of thermal analysis and calorimetry: vol. I: Principles and Practice, Elsevier, Amsterdam, 1998, pp. 509–546 (Chapter 12).
[22] Thermolab Instruction Manual: Evolved Gas Analyser for Thermal Analysis–Mass Spectrometry, Fisons Instruments, 37.
[23] Y. Narendar, G.L. Messing, Catal. Today 35 (1997) 247–268.
[24] Y. Narendar, G.L. Messing, Chem. Mater. 9 (1997) 580–587.
[25] K. Van Werde, D. Mondelaers, G. Vanhoyland, D. Nelis, M.K. Van Bael, J. Mullens, L.C. Van Poucke, B. Van der Veken, H.O. Desseyn, J. Mater. Sci. 37 (2002) 81–88.
[26] M. Rajendran, M.S. Rao, J. Solid State Chem. 113 (1994) 239–247.
[27] K. Van Werde, Ph.D thesis, Limburgs Universitair Centrum, Diepenbeek, 2003.
[28] O. Auciello, Integr. Ferroelectr. 15 (1997) 211–220.
[29] I. Koiwa, Y. Okada, J. Mita, A. Hashimoto, Y. Sawada, Jpn. J. Appl. Phys. 36 (1997) 5904–5907.
[30] T.-C. Chen, T. Li, X. Zhang, S.B. Desu, J. Mater. Res. 12 (8) (1997) 2165–2174.
[31] T.-C. Chen, T. Li, X. Zhang, S.B. Desu, J. Mater. Res. 12 (6) (1997) 1569–1575.
[32] A. Hardy, D. Mondelaers, M.K. Van Bael, J. Mullens, L.C. Van Poucke, G. Vanhoyland, J. D’Haen, J. Eur. Ceram. Soc., in press.
[33] CRC Handbook of Chemistry and Physics, eigthty-third ed., 2002–2003.
[34] M.K. Van Bael, D. Nelis, A. Hardy, D. Mondelaers, K. Van Werde, J. D’Haen, G. Vanhoyland, H. Van den Rul, J. Mullens, L.C. Van Poucke, F. Frederix, D.J. Wouters, Integr. Ferroelectr. 45 (2002) 113–122.